



# Broadband Shock-cell Noise Signature Identification Using a Wavelet-based Method

Lior Gefen, Carlos Pérez Arroyo, Roberto Camussi, Guillaume Puigt,  
Christophe Airiau

## ► To cite this version:

Lior Gefen, Carlos Pérez Arroyo, Roberto Camussi, Guillaume Puigt, Christophe Airiau. Broadband Shock-cell Noise Signature Identification Using a Wavelet-based Method. 22nd AIAA/CEAS Aeroacoustics Conference, May 2016, Lyon, France. pp.0, 10.2514/6.2016-2732 . hal-04109368

**HAL Id: hal-04109368**

**<https://hal.science/hal-04109368>**

Submitted on 30 May 2023

**HAL** is a multi-disciplinary open access archive for the deposit and dissemination of scientific research documents, whether they are published or not. The documents may come from teaching and research institutions in France or abroad, or from public or private research centers.


L'archive ouverte pluridisciplinaire **HAL**, est destinée au dépôt et à la diffusion de documents scientifiques de niveau recherche, publiés ou non, émanant des établissements d'enseignement et de recherche français ou étrangers, des laboratoires publics ou privés.



## Open Archive Toulouse Archive Ouverte (OATAO)

OATAO is an open access repository that collects the work of Toulouse researchers and makes it freely available over the web where possible.

This is an author-deposited version published in: <http://oatao.univ-toulouse.fr/>  
Eprints ID: 18312

**To cite this version:** Gefen, Lior and Pérez Arroyo, Carlos and Camussi, Roberto and Puigt, Guillaume and Airiau, Christophe  *Broadband Shock-cell Noise Signature Identification Using a Wavelet-based Method.* (2016) In: 22nd AIAA/CEAS Aeroacoustics Conference, 30 May 2016 - 1 June 2016 (Lyon, France)

Any correspondence concerning this service should be sent to the repository administrator:  
[staff-oatao@listes-diff.inp-toulouse.fr](mailto:staff-oatao@listes-diff.inp-toulouse.fr)

# Broadband Shock-cell Noise Signature Identification Using a Wavelet-based Method

L. Gefen\*      C. Pérez Arroyo†      R. Camussi ‡      G. Puigt§      C. Airiau¶  
*UniRoma3*      *CERFACS*      *UniRoma3*      *CERFACS*      *IMFT*

Civil and military aircraft manufacturers need to respond to increasingly more restrictive standards about noise emission. In order to fulfil those requirements the mechanisms underlying the noise production need to be understood. The supersonic jets at the exit of aircraft engines are known to contain several sources of noise, namely: screech (military aircrafts), Broadband Shock-cell Associated Noise (BBSAN) and large-scale structures. The current work is focused on the study of BBSAN by means of a wavelet-based technique. The technique was applied to a pressure nearfield line array for the sake of extracting the 'signatures' related to noise production mechanisms. Each 'signature' characterized by its shape and time-scale. The signature found up to approximately  $x/D = 6D$  has a 'wave-packet' like shape. The same shape is obtained at farfield locations for forward angles. The Sound Pressure Level (SPL) was computed using the nearfield signatures and it is in good agreement with the SPL computed using the pressure signals. The 'wave-packet' like shape 'signature' is associated to BBSAN as it has the same characteristics: same SPL and forward angles directivity.

## I. Introduction

The noise perceived in the aft-cabin for an aircraft at cruise condition is mainly due to the turbofan jet. The pressure mismatch between the ambient air and the secondary stream of a turbofan engine leads to the formation of (diamond-shaped) shock-cells. These series of expansion and compression waves interact with the vortical structures developing in the mixing layer of the jet. This interaction process generates intense noise components on top of the turbulent mixing noise, which makes supersonic jets noisier than their subsonic counterparts.<sup>1</sup> Supersonic jet noise is mainly composed of three components: the screech tonal noise, the broadband shock-associated noise (BBSAN) and the turbulent mixing noise. The first component is a tonal noise known as 'screech'. This tonal noise appears from a closed loop between the generation of vortical structures convected downstream and the perturbations propagated upstream that are generated when they interact with the shock-cell system. These perturbations will then interact with the development of the instabilities in the shear-layer closing a feedback loop. The screech phenomenon is usually generated by the interaction with the third and forth shock-cells.<sup>2</sup> The second component of supersonic jet noise is a broadband component known as BBSAN. The generation is based on the same interaction of the vortical structures as the screech, minus the feedback loop, as it was demonstrated experimentally by Tam *et al.*<sup>3</sup> The origin of the BBSAN was located by Norum *et al.*<sup>4</sup> in the downstream weaker shock-cells. The third component, the turbulent mixing noise of axisymmetric jets was analyzed by Tam *et al.*<sup>5</sup> who evidenced the existence of two universal similarity spectra, one for the noise generated by the large turbulent structures and the other for the fine-scale turbulence.

Several post-processing techniques in order to extract the different aerodynamic and aeroacoustic characteristics of the jets. In this paper, the wavelet-conditioning is applied to the numerical database in the present work. It is a wavelet-based post-processing technique used to detect energetic events in a signal.

\*PhD candidate, Universit Roma TRE, Dipartimento di Ingegneria, Via della Vasca Navale, 79, 00146 Roma, Italia.

†PhD candidate, CERFACS, Computational Fluid Dynamics, 42 avenue Coriolis, 31057 Toulouse CEDEX (France).

‡Full professor, Universit Roma TRE, Dipartimento di Ingegneria, Via della Vasca Navale, 79, 00146 Roma, Italia.

§Senior Researcher, CERFACS, Computational Fluid Dynamics, 42 avenue Coriolis, 31057 Toulouse CEDEX (France).

¶Full professor, Institut de Mécanique des Fluides de Toulouse, UMR 5502 CNRS/INPT-UPS, Allée du professeur Camille, Toulouse (France).

As seen in previous studies [6,7,8], the wavelet-conditioning is perfectly suitable for coherent-structures identification in jets. The identification is done by means of an energy criterion named Local Intermittency Measure<sup>9</sup> or LIM. By applying the technique to a signal at a specific location known to be greatly influenced by BBSAN, it is possible to isolate events due to BBSAN instead of those due to the turbulent-structures in the shear-layer.

In order to study BBSAN, an under-expanded single jet at Mach 1.15 is simulated with the Finite Volume multi-block structured solver *elsA* (Onera's software<sup>10</sup>). The acoustic farfield is calculated by the use of the Ffowcs-Williams & Hawkings analogy<sup>11</sup> (FWH). A wavelet-based post-processing method is then applied to nearfield pressure signals on a line array and to farfield pressure signals on a polar array.

At first, a description of the numerical simulation with *elsA* is given in section II. The description of the wavelet-based method is given in section III. In section IV the results are presented. The concluding remarks and perspectives are given in the last section V.

## II. Numerical Simulation

### A. Numerical Formulation

The full compressible Navier-Stokes equations are solved using the Finite Volume multi-block structured solver *elsA* (Onera's software<sup>10</sup>). The spatial scheme is based on the well-known Lele's implicit compact finite difference scheme of sixth-order,<sup>12</sup> extended to Finite Volumes by Fosso *et al.*<sup>13</sup> The above scheme is stabilized by the compact filter of Visbal & Gaitonde,<sup>14</sup> also used as an implicit subgrid-scale model for the present LES. Time integration is performed the six-step second-order Runge-Kutta DRP scheme of Bogey and Bailly.<sup>15</sup>

### B. Simulation Setup and Procedure

The case under investigation is the one of a cold supersonic under-expanded single jet, experimentally tested by André.<sup>16</sup> The jet is established from a convergent nozzle with exit diameter  $D = 38.0mm$  and a modeled nozzle lip thickness of  $0.125D$ . The nozzle is operated under-expanded at the stagnation to ambient pressure ratio  $p_s/p_\infty = 2.27$ . The Reynolds number,  $Re$ , based on the jet exit diameter is  $1.25 \times 10^6$  and the fully expanded jet Mach number is  $M_j = 1.15$ .

The numerical computation is initialized by a RANS simulation using the Spalart-Allmaras turbulence model.<sup>17</sup> The RANS solution is wall resolved in the inner and outer sections of the nozzle with a  $y^+ < 1$ . Once mesh convergence is achieved, the LES run is then initialized from the RANS simulation. The inner part of the nozzle is removed from the LES simulation and the RANS nozzle exit conservative variables are imposed.<sup>18</sup>

The boundary conditions are sketched in figure 1. Tam and Dong<sup>19</sup> non-reflective boundary conditions, extended to three dimensions by Bogey and Bailly<sup>20</sup> are used in the exterior inlet as well as in the lateral boundaries. The exit condition is based on the characteristic formulation of Poinsot and Lele.<sup>21</sup> Furthermore, sponge layers are coupled around the domain to attenuate exiting vorticity waves. Due to the fact that the interior of the nozzle is not modeled, no inflow forcing is applied at the exit of the nozzle to avoid parasite noise.

The simulation runs for 120 non-dimensional time units ( $\hat{t} = tD/c_\infty$ ) in order to reach statistically convergent results. After the transient phase, the simulation runs for  $\hat{t} = 140$ . The far-field sound is obtained by means of FWH analogy.<sup>11</sup> The surface used to propagate the variables to the far-field is located in a topological surface starting at  $r/D = 3.5$  from the axis and radially growing with the mesh. The cut-off mesh frequency is  $St \approx 2.0$ . In terms of frequency ( $St = fD/U_j$ ), this value is defined as  $f = c_\infty/(n\Delta)$ , where  $\Delta$  is the cell size,  $c_\infty$  the ambient speed of sound and  $n$  the number of cells needed to resolve fluctuations with the numerical scheme used. The sampling frequency has been set to 113,875Hz ( $St \approx 5.0$ ).

### C. Mesh Definition

The computational domain used for the LES simulation extends  $40D$  in the axial direction and  $7D$  in the radial direction using a butterfly block to avoid the singularity at the axis as it is shown in figure 2 (a) and (b). The mesh consists in  $75 \times 10^6$  cells with  $(1052 \times 270 \times 256)$  cells in the axial, radial and azimuthal

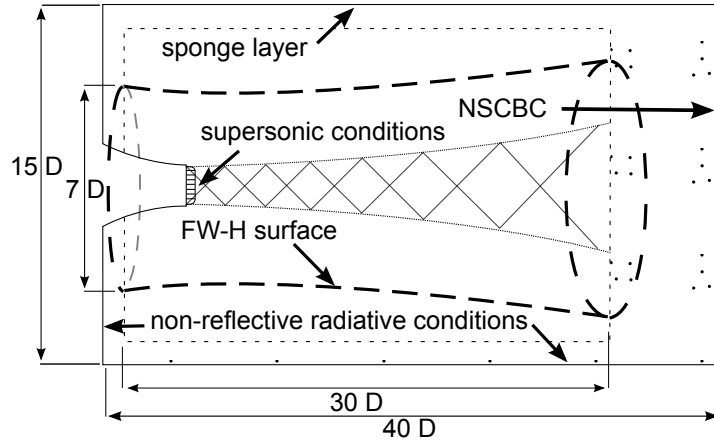


Figure 1. Sketch of the domain representing the different boundary conditions and dimensions.

directions respectively. The maximum expansion ratio between adjacent cells achieved in the mesh is less than 4%.

The mesh used in the LES simulation near the jet lip-line is coarsened in the radial direction with respect to the RANS mesh, meaning that no wall-resolution is achieved when the RANS solution is interpolated into the LES mesh. Nevertheless, the boundary layer at the exit of the nozzle is defined by 15 points. The radial discretization is shown for different  $x/D$  positions in figure 3 (a). Each single shock-cell is resolved within 40 cells in the axial direction. The axial discretization is shown in figure 3 (b).

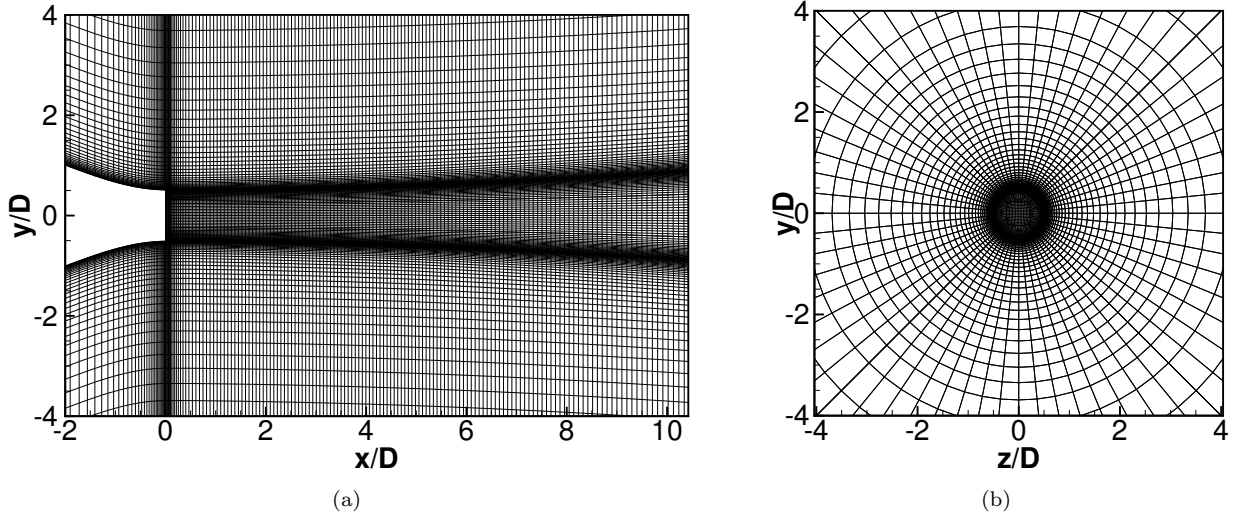


Figure 2. Mesh cuts representing 1 every 4 cells in the plane (a)  $z/D = 0$  and the plane (b)  $x/D = 0$

### III. Wavelet-based method

The wavelet-conditioning, presented in this section, is used on the numerical database. The technique is first applied to a pressure nearfield line array at  $r/D = 3D$  following an angle of 5 degrees, and then to a pressure farfield polar array with  $\theta \in [20^\circ, 160^\circ]$ . In III.A a short introduction to wavelets is given. The procedure by which the events are selected is described in III.B. Finally, the conditional-average is explained in III.C.

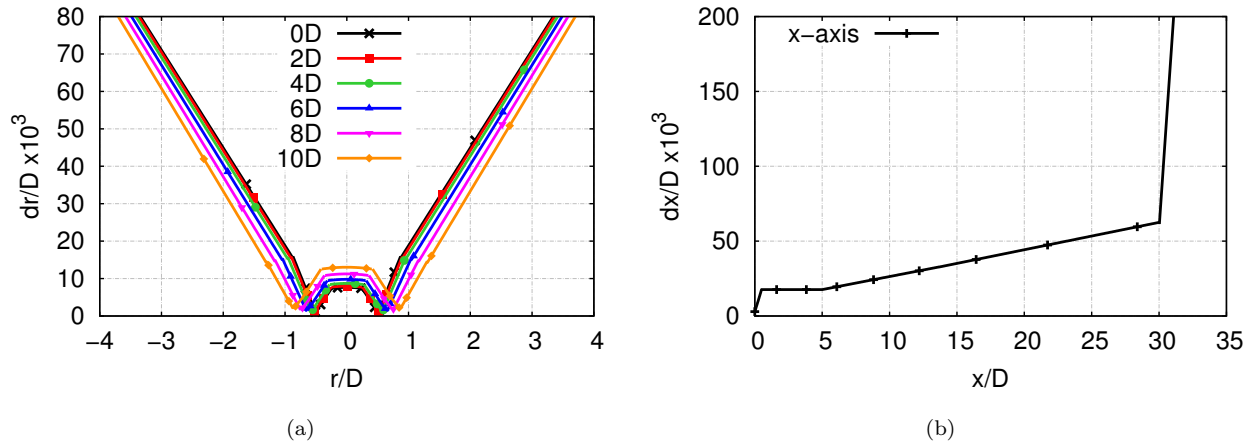


Figure 3. Discretization of the mesh along (a) the radial distribution for different  $x/D$  positions and (b) the axial distribution on the axis

### A. Short-introduction to Wavelets

The Fourier-Transform is the usual method used to study the frequency content of a certain signal and allows to exclusively study the signal in its frequency domain losing the time-information. The Short-Time Fourier Transform (STFT) is an alternative that allows to obtain a frequency-time representation of the signal. The STFT is FT applied on a sliding window instead of the entire signal. The main drawback of STFT is time-length of the chosen window. This limitation is due to the uncertainty principle or Heisenberg's principle. The time-length of the window will influence the resolution of the decomposition: a larger window in time will give a better decomposition at low frequency while in counterpart will have a poorer resolution at higher frequency and viceversa.

As for the two former techniques, the wavelet-transform is ruled by the uncertainty principle. However, because the wavelet-transform is a multi-scale transform, the uncertainty principle does not affect it as it does for the FT and the STFT. The Continuous Wavelet-Transform formulation is given by:

$$w(s, \tau) = \frac{1}{\sqrt{|s|}} \int_{-\infty}^{+\infty} p(t) \overline{\Psi}\left(\frac{t-\tau}{s}\right) dt, \quad (1)$$

where  $p(t)$  is the time-signal to analyse,  $\{w(s, \tau)\}$  is the set of wavelet coefficients,  $\tau$  is the translation parameter,  $s$  is the dilatation parameter also called scale parameter and  $\overline{\Psi}\left(\frac{t-\tau}{s}\right)$  is the complex-conjugate of the daughter-wavelet  $\Psi\left(\frac{t-\tau}{s}\right)$  obtained by the translation and dilatation of the so-called mother-wavelet  $\Psi(t)$ . The scale of the wavelet-transform is as the window for STFT which means that each scale will correspond to a different size of window. For further information about the Wavelet-Transform the reader can refer to [9,22].

### B. Energetic events selection

The wavelet-conditioning already presented in the introduction is a well-assessed technique for coherent-structures identification in subsonic flows [6,7,23,8,24]. In the present work, the technique is used at a specific spatial location, close to the nozzle exit, in order to isolate the contribution from BBSAN. A comparison is done with the signature emitted by the coherent-structures at a farther axial location and then with the farfield signatures.

Wavelet-conditioning is based on the so-called Local Intermittency Measure or LIM, introduced by Farge,<sup>9</sup> which gives a local measure of the ratio between local energy and the time-averaged for a specific scale  $s$ . The LIM's mathematical formulation, noted  $L(s, \tau)$ , is:

$$L(s, \tau) = \frac{w^2(s, \tau)}{\langle w^2(s, \tau) \rangle_\tau}, \quad (2)$$

where  $w^2(s, \tau)$  is the local energy for a specific time and scale, and  $\langle \bullet \rangle_t$  represents a time average. The value of the LIM gives an indication about the fluctuation of the energy. It is possible to select the most energetic

events in a signal  $p(t)$  by selecting a proper threshold  $T$  with the conditions:

$$\left\{ \begin{array}{l} L(s, \tau) > T, \\ \frac{\partial L}{\partial \tau}(s, \tau) = 0, \\ \frac{\partial^2 L}{\partial \tau^2}(s, \tau) < 0, \end{array} \right. \quad (3)$$

that define local maxima of  $L(s, \tau)$ . This set, labeled later  $P_k$ , is going to be used in the next paragraph for the conditional-average. The value of the threshold was chosen to be 1 in order to increase the number of events selected as the time-length of the signal on which the analysis is performed is short.

### C. Conditional-average

The outcome of the previous explained procedure is a set of times belonging to the energetic events which are energetic peaks in the analysed signal. At each time location corresponding to a peak of energy it is possible to extract a window  $W$ , of fixed time-length  $t_W$ , from the original signal  $p(t)$ . The conditional-average,  $\tilde{p}$  can be calculated from this set of windows:

$$\tilde{p}_m^n(W) = \langle p_m | P_k \rangle_{\tilde{\tau}_s^n} = \frac{1}{N^n} \sum_{i=1}^{N^n} p_m(\xi_i), \quad (4)$$

where the superscript  $n$  and subscript  $m$  stand for the position of the reference signal and of any other signal of the array, respectively, the subscript  $s$  stands for the scale,  $N^n$  is the number of detected events,  $\tilde{\tau}_s^n$  is the set of corresponding times for a specific scale  $s$  at which these events are occurring and  $\{\xi_i\}$  is the interval surrounding each peak,  $\xi_i \in [\tilde{t}_i - \frac{t_W}{2}, \tilde{t}_i + \frac{t_W}{2}]$ ,  $\tilde{t}_i \in \tilde{\tau}_s^n$ .

As LES is really expensive and long to produce, most of the time the resulting simulations of a certain flow are limited to few instants. The short time-length has an impact on the number of events that can be selected. In order to improve the results, the formulation of the conditional-average in equation 4 is modified. First, a multiplicative coefficient is introduced to the sum of equation 4 because the LIM does not give any indication about the sign (positive or negative) of the peak in the real domain. This multiplicative coefficient is  $sign(p_n(\tilde{t}_i)) = p_n(\tilde{t}_i)/|p_n(\tilde{t}_i)| = \pm 1$ . A first post-processing with the wavelet-conditioning is accomplished by doing the conditional-average on positive or negative peaks separately. The results are similar but out of phase by  $\pi$ . In addition, a second average is computed azimuthally. By applying the same methodology on each azimuthal location available, it is then possible to compute an azimuthally-averaged conditional-average at each axial position. The new formulation of the conditional-average is:

$$\tilde{p}_m^n(W) = \langle p_{m,\theta} | P_k \rangle_{\tilde{\tau}_{s\theta}^n} = \frac{1}{N^n \cdot N_\theta} \sum_{j=1}^{N_\theta} \sum_{i=1}^{N^n} sign(p_{n,j}(\tilde{t}_{i,j})) p_{m,j}(\xi_{i,j}), \quad (5)$$

where  $N_\theta$  is the number of azimuthal locations. The conditional-average can be performed on a signal  $p_n$  by using its own set of times  $\tilde{\tau}_s^n$ , and so  $n = m$ : this is the auto-conditioning. It is also possible to perform the conditional-average of a signal  $p_m$  by using the times of a signal  $p_n$ , and so  $n \neq m$ : it is then called cross-conditioning. The auto/cross-conditioning are presented on figure 4: the top is the auto-conditioning where the selection of  $W$  is done in the reference signal  $n$ ; and the bottom is the cross-conditioning of another signal  $m$  where  $W$  is centered around the times obtained with signal  $n$ . The results of the conditional-average will be denoted as the signature obtained with the wavelet-conditioning and will be only referred by signature. Next, the results are presented with first an acoustic characterization of the jet.



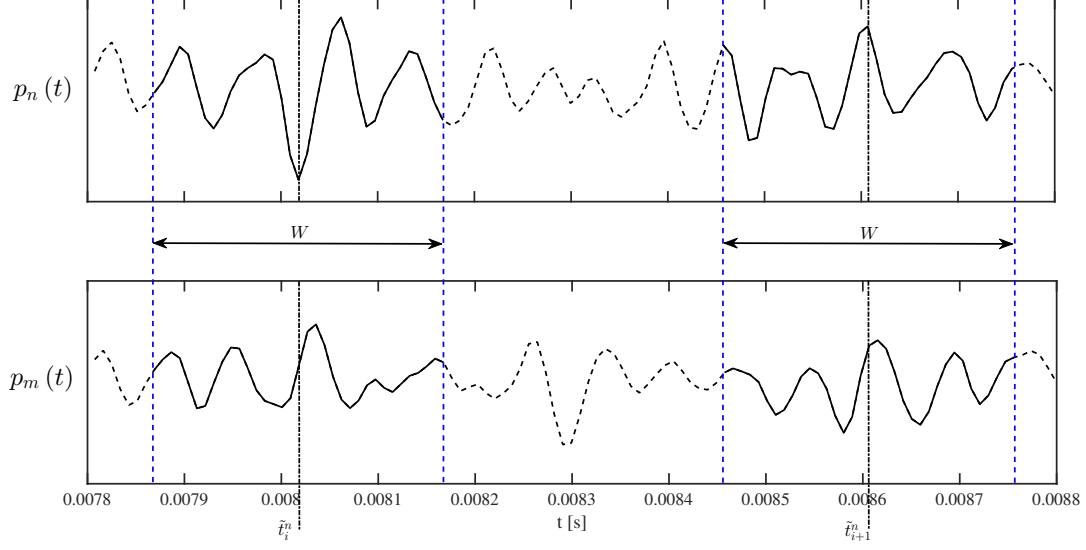


**Figure 4.** *Auto-conditioning of a signal  $p_n(t)$  and cross-conditioning of a signal  $p_n(t)$*

## IV. Results

### A. Acoustic characterization

The auto-correlation of nearfield pressure signals are performed and depicted in figure 5. The pressure signals are located on a line array at a radial distance of  $r/D = \{1, 2, 3\}$  and inclined by 5 degrees. Different phenomena can be observed in the vicinity of the nozzle exit and further downstream. The correlations in the vicinity of the nozzle are enhanced with increasing radial distance because of the reduction of the hydrodynamic component. The correlations have a 'wave-packet' like shape their characteristic time is decreasing with increasing axial distance up to approximately  $7D$  for figure 5 (b) and (c). The denomination wave-packet here is exclusively related to the shape and has nothing to do with the wave-packet model used in subsonic jets as a source model for large turbulent-structures.

The BBSAN, that is mainly being generated at the position range  $7 < x/D < 10$  where the latest shock-cells are located, is visible in the nearfield for  $x/D < 7$ . Figure 6 shows the Sound Pressure Level (SPL) along the same position of figure 5. The BBSAN appears as it was shown by Savarese<sup>25</sup> as a 'banana shaped' contour. The effect of the cut-off Strouhal that depends on the cell size is clearly visible. While the maximum Strouhal is reduced for higher  $r/D$  positions, the hydrodynamic component at low frequencies is reduced as well. Therefore, the positions  $x/D = \{2.5, 6.2\}$  and  $r/D = 3$ , highlighted with the dashed circle, will be a point of interest in the following sections along with the position  $x/D = 14$  for comparison.

Subsequently to the correlation and nearfield analysis it was decided to apply the wavelet-conditioning on the line array at  $r = 3D$  because it is the position at which the hydrodynamic noise is minimum in the vicinity of the nozzle exit.

The pressure perturbations are propagated to the farfield (50 diameters) by means of the FWH analogy using the flow values on a topological surface located at  $r/D = 3$ . The results are shown in figure 7 (a) at different angles and compared with the experimental results of André.<sup>16</sup> The results are in good agreement up to the cut-off Strouhal. However, no screech was detected by the simulation due to the fact that no interior of the nozzle is modeled.<sup>26</sup> Without it, the instabilities inside the shear-layer develop half a diameter downstream after a laminar region. Having the instabilities closer to the nozzle exit might help the presence of screech phenomenon as well, increasing the feedback loop gain because the lip acts as a reflecting boundary for the perturbations traveling upstream.<sup>27</sup> The OverAll Sound Pressure Level (OASPL) is computed in the audible range [20 - 20000 Hz] and compared with the experimental results in figure 7 (b).



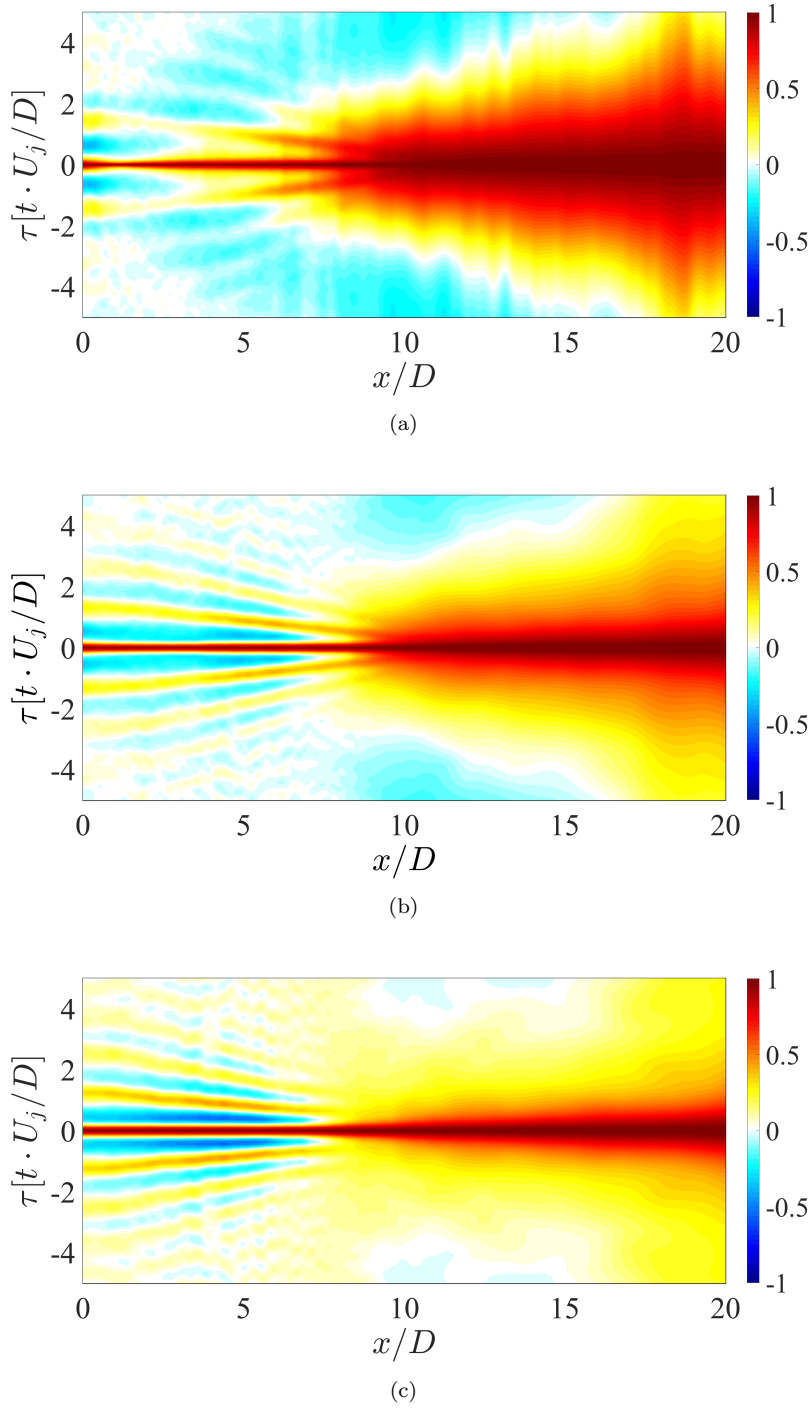


**Figure 5.** *Auto-correlation of pressure signals of a linear-array of probes at  $r/D = \{1, 2, 3\}$ .*

## B. Wavelet-conditioning

The methodology described in section III is applied to pressure signals on a nearfield line array at 3D and on a farfield polar array. Morlet's wavelet with a central frequency of  $\omega_0 = 6$  is used for the detection of the energetic events.

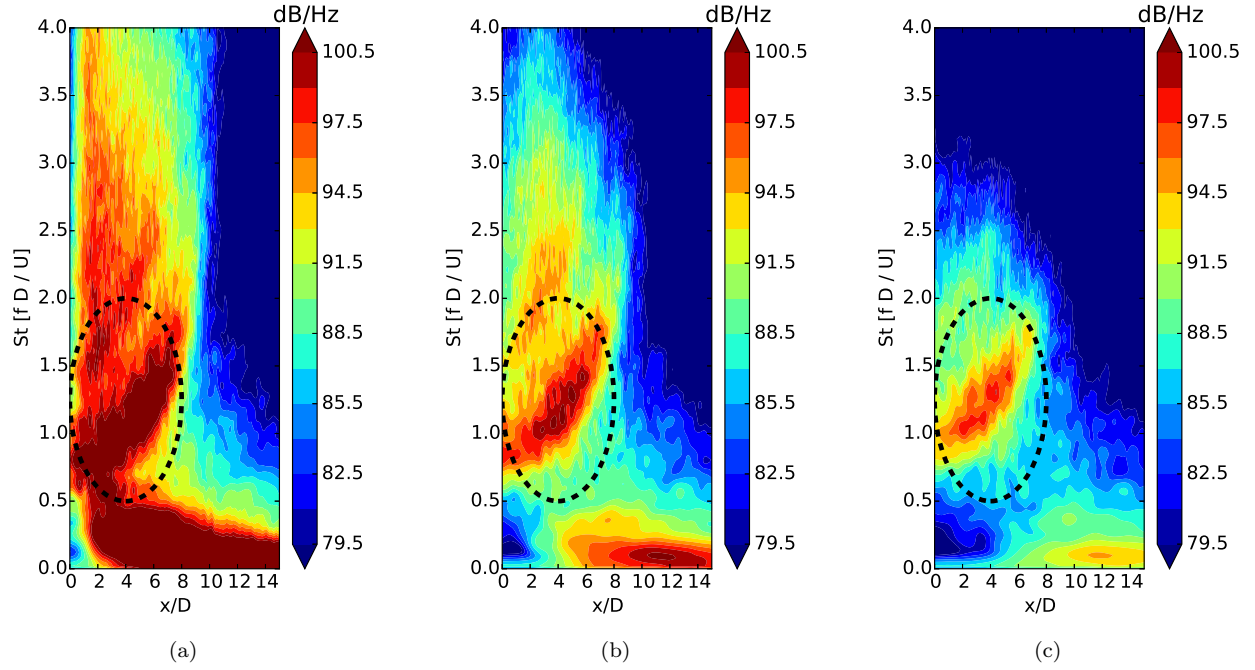


Figure 6. Nearfield SPL in dB/Hz along different axial positions for a line array with an angle of  $5^\circ$  at (a)  $r/D = 1$ , (b)  $r/D = 2$  and (c)  $r/D = 3$ .

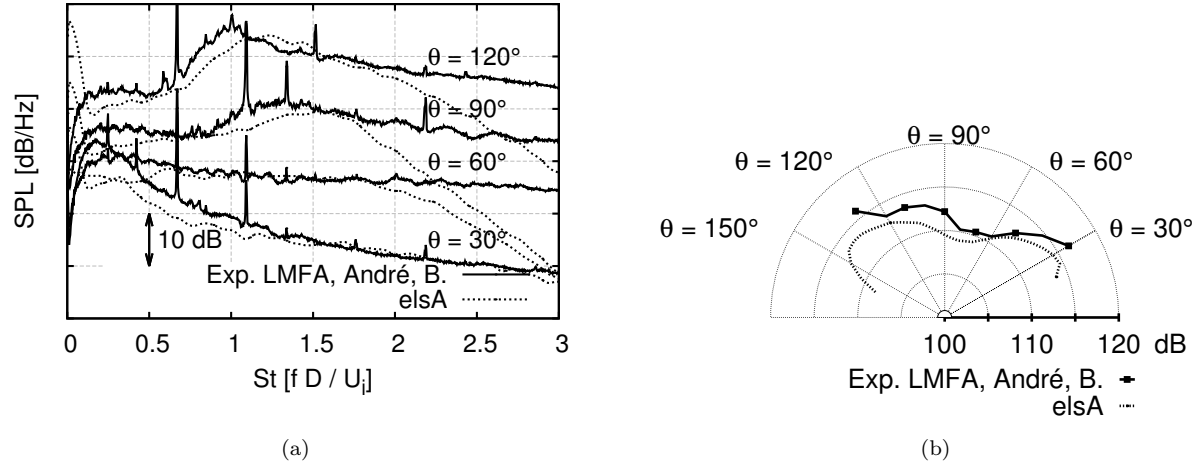
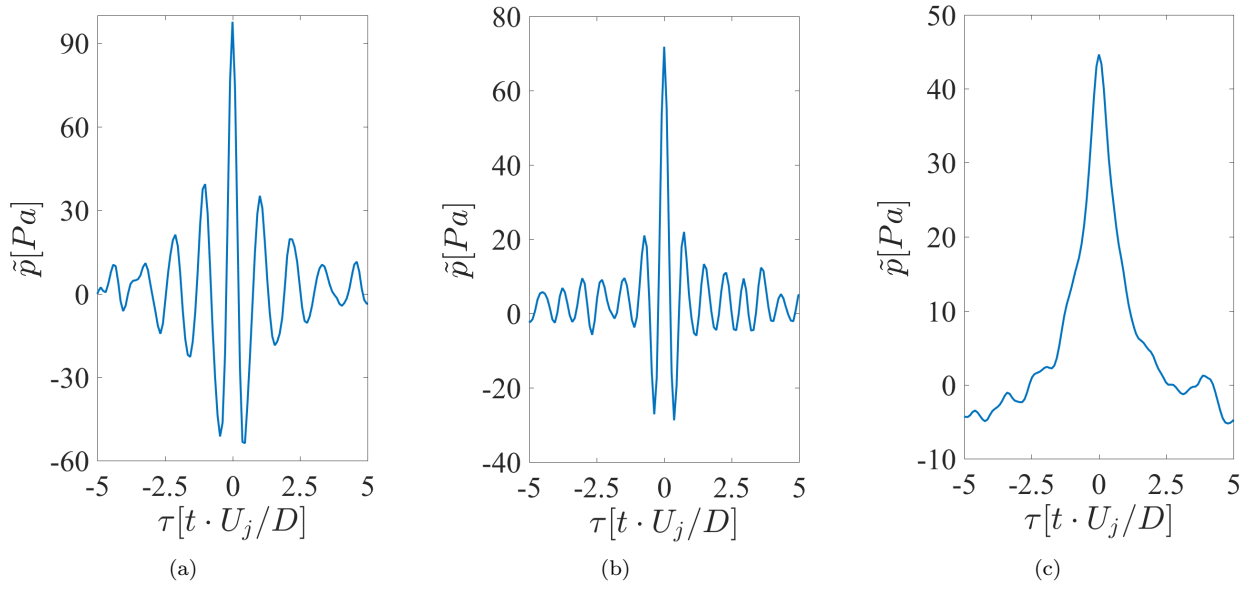


Figure 7. Acoustic spectrum in the farfield (50 diameters) for a  $M_j = 1.15$  under-expanded jet.  $\theta$  is measured with respect to the jet axis, (a) SPL, (b) OASPL.

### 1. Nearfield line array

The wavelet-conditioning is applied first to the nearfield line array in order to bring-up BBSAN presence at axial positions close to the nozzle exit. It is observed for  $x/D \in [0, 5.5]$  that the signatures' shape, obtained with the conditional-averaged process, is similar to the shape of the auto-correlation at the same axial locations. For brevity, only the results at axial location  $x/D = \{2.5, 6.2, 14\}$  are presented here. Figure 8 shows the auto-conditioning of the signals at these positions. It is clear that there are two different phenomena, one observed close to the nozzle exit and the second further downstream. The ones close to the nozzle exit depict oscillations while the one downstream is a single peak.

In figure 9, each subplot represents a map of the cross-conditioning with the reference signals at  $x/D = \{2.5, 6.2, 14\}$ . The cross-conditioning is done with the signals comprised within  $4D$  from the reference signal,



**Figure 8.** *Auto-conditioning of pressure signal of the nearfield line array at (a)  $x/D = 2.5$ , (b)  $x/D = 6.2$ , (c)  $x/D = 14$ .*

for instance: the reference signal at  $x/D = 2.5$  and the close signals at  $x/D \in [0.5, 4.5]$ . A dashed line is plotted on each subplot of figure 9 to highlight the sense in which the selected events are travelling. Figure 9 (a) shows that the events seem to travel counter-stream, that is, from downstream locations to upstream locations. On the other hand, on subplot 9 (c) the structure is evolving with the flow stream. Subplot 9 (b) depicts the transition between the two previous subplots as both phenomena can be observed.

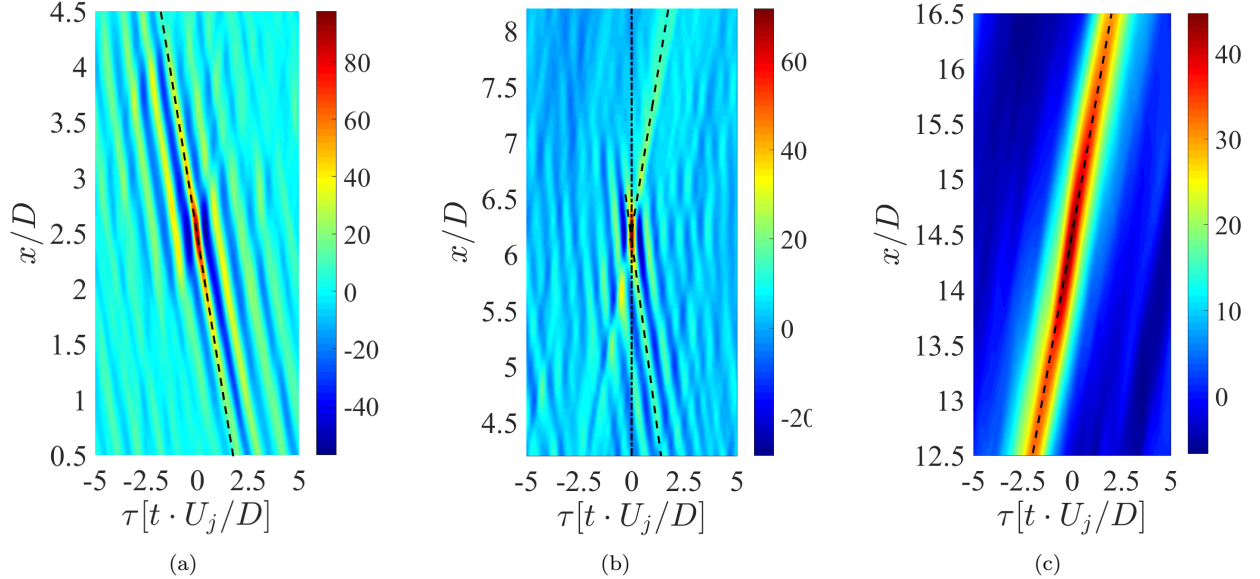


**Figure 9.** *Auto/cross-conditioning of pressure signal of the nearfield line array at (a)  $x/D = 2.5$ , (b)  $x/D = 6.2$ , (c)  $x/D = 14$ .*

The SPL of the different signatures from the previous figure is showed in figure 10. The SPL results are scaled in order to qualitatively match the result in figure 6 (c). Despite the fact that the SPL level is different (the computation is done on a far smaller number of samples), the representation seems to match the one found in figure 6 (c) and so the wavelet-conditioning allows to preserve the main feature of the flow.

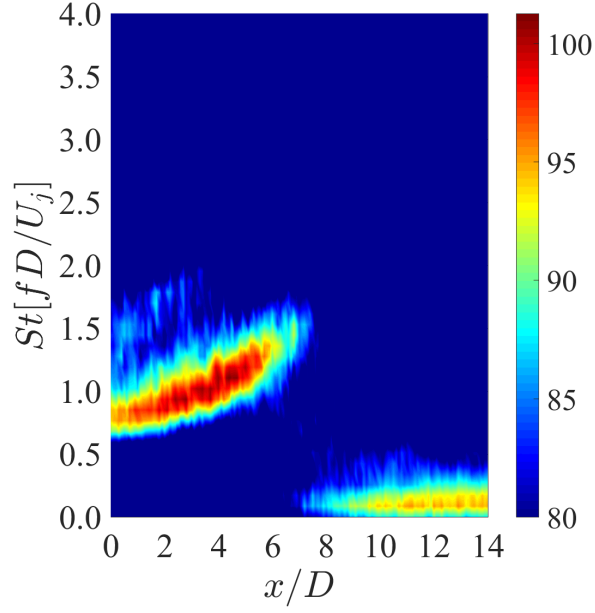


**Figure 10.** *SPL of the auto-conditioned signal at each nearfield location on the line array at  $r/D = 3D$ .*

## 2. Farfield polar array

In the current section the results obtained with the wavelet-conditioning applied to the farfield polar array are presented. Only the results obtained for  $\theta = \{30, 90, 120\}$  are presented here. The signatures for the three chosen polar angles are shown in figure 11. As for the nearfield results, it is observed that there is different phenomena ruling the downstream and upstream acoustic field.

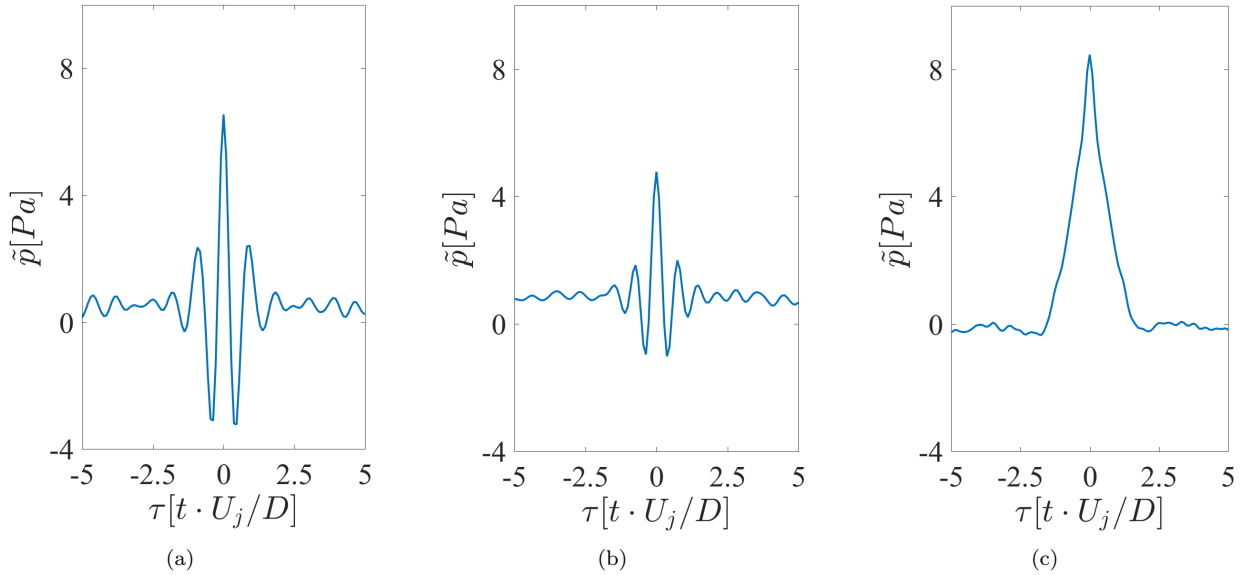


**Figure 11.** *Auto-conditioning of farfield pressure at (a)  $\theta = 120$ , (b)  $\theta = 90$ , (c)  $\theta = 30$ .*

Figures 11.(a) and 11 (b) have a similar signature's shape and are similar to those in figures 6 (a) and 6 (b). The signature in figure 6 (a) slightly deviates from figures 11.(a) and 11 (b) as it presents more oscillations due to the fact that it is closer to the nozzle exit.

Nevertheless, the signatures are similar between nearfield and upstream farfield angles. As it is known that

BBSAN is radiating in upstream angles with a strong directivity,<sup>3</sup> the signatures found with the wavelet-conditioning can be associated with BBSAN emission. The amplitude of the signature at  $90^\circ$  is lower than the one at  $120^\circ$ . This is in agreement with the widening and decreasing in amplitude of the BBSAN peak at upstream angles.

## V. Conclusion

The simulation of an under-expanded single jet at Mach 1.15 is performed. First, the nearfield is studied by means of the cross-correlation at each axial position for the different radial distances. Second, its acoustic characterisation is studied by means of SPL plots obtained in the nearfield at different radial distances,  $r/D = \{1, 2, 3\}$ . Good agreement is found with experimental results in the literature. The auto-correlation and nearfield acoustic characterisation results were used in order to choose the radial distance at which the wavelet-conditioning is performed. Next the wavelet-conditioning is applied to the nearfield line array at  $r/D = 3$  with a spreading angle of 5 degree and to the farfield polar array. The nearfield signature at  $x/D = 2.5$  is compared to the one at  $x/D = 14$ . The signatures are different and so the phenomena captured. Then, the nearfield signatures are compared to the farfield signatures. The signatures at  $x/D = \{2.5, 6.2\}$  are similar in shape to those at  $\theta = \{90^\circ, 120^\circ\}$  where BBSAN is known to radiate the most. In addition, the SPL of the signatures is computed and compared to the SPL obtained with the pressure signals. Good qualitative agreement is found between them. The signatures in the nearfield are compared to those obtained at farfield positions. Both signatures are similar in shape for the upstream and downstream directions.

To conclude, it is shown that the wavelet-conditioning is a post-processing technique capable to capture the broadband shock-cell associated noise features at the nearfield and at the farfield.

## Acknowledgments

This research project is supported by a Marie Curie Initial Training Networks (ITN) AeroTraNet 2 of the European Community's Seventh Framework Programme (FP7) under contract number PITN-GA-2012-317142 that aims to generate a ready-to-use model for shock-cell noise characterization. The authors are thankful to Onera for licensing CERFACS to use the code *elsA*.

## References

- <sup>1</sup>Tam, C. K., "Supersonic jet noise," *Annu. Rev. of Fluid Mech.*, Vol. 27, No. 1, 1995, pp. 17–43.
- <sup>2</sup>Krothapalli, A., Hsia, Y., Baganoff, D., and Karamcheti, K., "The role of screech tones in mixing of an underexpanded rectangular jet," *J. Sound Vib.*, Vol. 106, No. 1, 1986, pp. 119–143.
- <sup>3</sup>Tam, C. and Tanna, H., "Shock associated noise of supersonic jets from convergent-divergent nozzles," *J. Sound Vib.*, Vol. 81, No. 3, 1982, pp. 337–358.
- <sup>4</sup>Norum, T. and Seiner, J., "Broadband shock noise from supersonic jets," *AIAA J.*, Vol. 20, No. 1, 1982, pp. 68–73.
- <sup>5</sup>Tam, C. K., Golebiowski, M., and Seiner, J. M., "On the two components of turbulent mixing noise from supersonic jets," *2nd AIAA/CEAS Aeroacoustics Conference, May 6-8, 1996/State College, PA*, American Institute of Aeronautics and Astronautics, 1996.
- <sup>6</sup>Camussi, R. and Guj, G., "Orthonormal wavelet decomposition of turbulent flows: intermittency and coherent structures," *Journal of Fluid Mechanics*, Vol. 348, 1997, pp. 177–199.
- <sup>7</sup>Camussi, R. and Guj, G., "Wavelet decomposition and coherent structures eduction of low Re turbulent hot wire signals," *Applied Scientific Research*, Vol. 57, 1997, pp. 195–209.
- <sup>8</sup>Camussi, R., "Coherent Structures identification from wavelet analysis of particle image velocimetry data," *Experiments in Fluids*, Vol. 32, 2002, pp. 76–86.
- <sup>9</sup>Farge, M., "Wavelet Transforms and Their Applications to Turbulence," *Annual Review of Fluid Mechanics*, Vol. 24, 1992, pp. 395–457.
- <sup>10</sup>Cambier, L., Heib, S., and Plot, S., "The Onera elsA CFD software: input from research and feedback from industry," *Mech. & Ind.*, Vol. 14, No. 03, 2013, pp. 159–174.
- <sup>11</sup>Farassat, F. and Succi, G. P., "The prediction of helicopter rotor discrete frequency noise," *American Helicopter Society, Annual Forum, 38th, Anaheim, CA, May 4-7, 1982, Proceedings.(A82-40505 20-01) Washington, DC, American Helicopter Society, 1982, p. 497-507.*, Vol. 1, 1982, pp. 497–507.
- <sup>12</sup>Lele, S., "Compact finite difference schemes with spectral-like resolution," *J. Comput. Phys.*, Vol. 103, 1992, pp. 16–42.
- <sup>13</sup>Fosso-Pouangue, A., Deniau, H., Sicot, F., and Sagaut, P., "Curvilinear Finite Volume Schemes using High Order Compact Interpolation," *J. Comput. Phys.*, Vol. 229, No. 13, 2010, pp. 5090–5122, jx.
- <sup>14</sup>Visbal, M. and Gaitonde, D., "On the Use of Higher-Order Finite-Difference Schemes on Curvilinear and Deforming Meshes," *J. Comput. Phys.*, Vol. 181, 2002, pp. 155–185.

- <sup>15</sup>Bogey, C. and Bailly, C., “A family of low dispersive and low dissipative explicit schemes for flow and noise computations,” *J. Comput. Phys.*, Vol. 194, No. 1, 2004, pp. 194–214.
- <sup>16</sup>André, B., Castelain, T., and Bailly, C., “Broadband Shock-Associated Noise in Screeching and Non-Screeching Under-expanded Supersonic Jets,” *AIAA J.*, Vol. 51, No. 3, 2013, pp. 665–673.
- <sup>17</sup>Spalart, P. and Allmaras, S., “A one-equation turbulence model for aerodynamic flows,” *AIAA Paper 92-0439, 30th Aerospace Sciences Meeting and Exhibit, Reno, Nevada (1992)*, 1992.
- <sup>18</sup>Shur, M. L., Spalart, P. R., Strelets, M. K., and Garbaruk, A. V., “Further steps in LES-based noise prediction for complex jets,” *44th AIAA Aerospace Sciences Meeting and Exhibit, 9 - 12 January 2006, Reno, Nevada, AIAA Paper 2006-485*, Vol. 485, 2006, p. 2006.
- <sup>19</sup>Tam, C. and Dong, Z., “Radiation and outflow boundary conditions for direct computation of acoustic and flow disturbances in a nonuniform mean flow,” *J. Comput. Phys.*, Vol. 4, No. 02, 1996, pp. 175–201.
- <sup>20</sup>Bogey, C. and Bailly, C., “Three-dimensional non-reflective boundary conditions for acoustic simulations: far field formulation and validation test cases,” *Acta Acust.*, Vol. 88, No. 4, 2002, pp. 463–471.
- <sup>21</sup>Poinsot, T. and Lele, S., “Boundary Conditions for Direct Simulations of Compressible Viscous Flows,” *J. Comput. Phys.*, Vol. 101, 1992, pp. 104–129.
- <sup>22</sup>Antoine, J.-P., Murenzi, R., Vandergheynst, P., and Twareque Ali, S., *Two-Dimensional Wavelets and their Relatives*, Cambridge University Press, 2004.
- <sup>23</sup>Guj, G. and Camussi, R., “Statistical analysis of local turbulent energy fluctuations,” *Journal of Fluid Mechanics*, Vol. 382, 1999.
- <sup>24</sup>Guj, G., Carley, M., and Camussi, R., “Acoustic Identification of coherent structures in a turbulent jet,” *Journal of Sound and Vibration*, Vol. 259, 2003, pp. 1037–1065.
- <sup>25</sup>Savarese, A., Jordan, P., Girard, S., Royer, A., Fourment, C., Collin, E., Gervais, Y., and Porta, M., “Experimental study of shock-cell noise in underexpanded supersonic jets,” *AIAA J.*, 2013.
- <sup>26</sup>Berland, J., Bogey, C., and Bailly, C., “Large eddy simulation of screech tone generation in a planar underexpanded jet,” *12th AIAA/CEAS Aeroacoustics Conference (27th AIAA Aeroacoustics Conference 8–10 May 2006, Cambridge, Massachusetts)*, 2006, pp. 8–10.
- <sup>27</sup>Norum, T., “Screech suppression in supersonic jets,” *AIAA J.*, Vol. 21, No. 2, 1983, pp. 235–240.